A new perspective on the flame describing function of a matrix flame

Maria Heckl

Department of Mathematics, Keele University, Staffordshire ST5 5BG, U.K.

(Submission date: August 30, 2013; Revised Submission date: May 12, 2014; Accepted date: August 04, 2014)

ABSTRACT

This paper considers a fundamental thermoacoustic test rig developed by Noiray ("Linear and nonlinear analysis of combustion instabilities, application to multipoint injection systems and control strategies", PhD thesis, École Centrale Paris, 2007) and models it with an entirely analytical approach. The test rig is treated as a system of two coupled elements: an acoustic resonator and a flame with oscillating rate of heat release. We describe the acoustics of the combustion rig in terms of modes, and derive a governing equation for one such mode. This turns out to be the equation for a damped harmonic oscillator, forced by the heat release rate from the flame. In order to model the heat release rate, and in particular its nonlinear aspects, we develop a generalised $n\tau$-law with amplitude-dependent coefficients and multiple time-lag. The coefficients are determined from Noiray's measured flame describing function. Stability predictions are made by evaluating the sign of the damping coefficient in the governing equation. These predictions are in excellent qualitative agreement with the measured stability behaviour. Finally, the physical mechanisms of the amplitude-dependence are explored.

1. INTRODUCTION

If a flame is situated inside or near an acoustic resonator, thermoacoustic instabilities can arise due to a feedback between the acoustic field and the rate of heat released from the flame. The pressure amplitudes involved in such instabilities tend to be very high, and in extreme cases, they cause serious hardware damage. Several kinds of combustion systems (such as gas turbines for electricity generation, domestic boilers, furnaces and rocket engines) are prone to suffer such instabilities. Particularly prone, unfortunately, are new combustion technologies designed to minimise pollutant emission. Their development is hampered by thermoacoustic instabilities, which can occur spontaneously and are the topic of intense world-wide research. Reviews of this research can be found, for example, in [1-5].

*Corresponding author: Maria Heckl [m.a.heckl@keele.ac.uk]

A widely used tool for modelling the interaction between the heat release rate from a flame and velocity fluctuations at the burner outlet is the *flame transfer function* (FTF). It is the ratio in the frequency domain of the non-dimensional rate of heat release $\hat{Q}(\omega)/\bar{Q}$ to the non-dimensional acoustic velocity $\hat{u}(\omega)/\bar{u}$. It can be measured for a given combustion system by imposing a harmonic velocity perturbation and measuring the resulting heat release rate, and doing so for a range of frequencies. The FTF is a linear concept. It can be extended into the nonlinear domain by measuring the FTF spectrum for several velocity amplitudes, thus creating a family of curves along the frequency axis. This is called the *flame describing function* (FDF), and we denote it by $\mathcal{T}(\omega, A)$, where A is the velocity amplitude,

$$\frac{\hat{Q}(\omega)}{\bar{Q}} = \mathcal{T}(\omega, A)\frac{\hat{u}(\omega)}{\bar{u}}. \tag{1.1}$$

The FDF has become an established tool for modelling nonlinearities in the thermoacoustic interaction. It has been used by several researchers, such as the EM2C Group at École Centrale Paris [6, 7, 8], by Dowling [9, 10] and others [11, 12].

The simplest way to describe the flame-acoustic interaction is the $n\tau$-law, which is

in the time domain:
$$\frac{Q(t)}{\bar{Q}} = n\,\frac{u(t-\tau)}{\bar{u}}, \tag{1.2}$$

in the frequency-domain:
$$\frac{\hat{Q}(\omega)}{\bar{Q}} = n\,\mathrm{e}^{\mathrm{i}\omega\tau}\,\frac{\hat{u}(\omega)}{\bar{u}}. \tag{1.3}$$

n is the *interaction index*, which is a measure for the coupling between the flame and the acoustic wave; τ is a *time-lag* associated with the propagation of convected disturbances in the flow. The $n\tau$-law was introduced in the 1950s by Crocco [13] to model instabilities in rocket motors. It has since then been used by many researchers to model a multitude of combustion systems [14]. The $n\tau$-law has also been extended into the nonlinear domain by Hield et al [15], who studied a bluff-body flame and proposed that both n and τ depend on amplitude.

In this paper we consider a *matrix flame*. This type of flame involves a perforated plate with a premixed gas flowing through the holes in the plate. Downstream of each hole, a conical flame is anchored, giving rise to a two-dimensional array, i.e. a matrix, of small flames close to the plate. The complete flame surface consists of conical regions (above the holes in the plate) and of flat regions (above the solid parts of the plate). The behaviour of matrix flames differs from that of other flames, even from that of a single conical flame. The most notable features in the FTF spectrum of a matrix flame are [16]

- excess gain (i.e. a band in the low-frequency range where the gain has values above 1)
- a phase that increases linearly with frequency (at least in the low-frequency range), indicating that there is a distinct time-lag
- low-pass filter behaviour.

Matrix flames exposed to high excitation amplitudes exhibit flame pinching, as has been observed for example in [17, 18].

Noiray et al. [6, 18, 19] performed a fundamental study of a particular laboratory burner comprised of a resonant cavity and a matrix flame. For this burner, they developed a theoretical model with two key elements. One element is a linear description of the resonant cavity in terms of classical duct acoustics. The other element is the description of the flame dynamics, which is done with the measured FDF. The two elements are then combined into a comprehensive model, which yields predictions of the linear and nonlinear stability behaviour as well as limit cycle amplitudes.

Our paper follows in the footsteps of this work and has the same two elements: one for the flame dynamics and one for the acoustic resonator. For the flame dynamics, we construct an FDF, which has the form of a generalised $n\tau$-law with amplitude-dependent parameters. The amplitude-dependence is inferred from the measured FDF in [6, 19]. In order to describe the acoustic resonator, we use a Green's function approach. We assume that the acoustic modes are uncoupled and derive the governing equation for an individual mode. This equation turns out to be that of a damped harmonic oscillator, forced by the fluctuating heat release rate. We combine the model for the flame with that for the acoustic resonator and then obtain a homogeneous (i.e. unforced) equation of motion for each mode. This equation has the same form as that of a simple damped oscillator. The damping coefficient turns out to be amplitude-dependent, and thus it is straightforward to predict the linear and nonlinear stability behaviour for different excitation amplitudes and other system parameters.

The same combustion system has been studied in a forerunner [20] of the current paper. In [20] the nonlinearity in the flame model was limited to an amplitude-dependent time-lag. With this flame model it was possible to predict some of the observed nonlinear behaviours correctly, but not all. In particular, the results for the limit cycle amplitudes differed qualitatively from the observed behaviour.

In this current paper, the flame model is improved by including a second type of nonlinearity: the gain-maximum (a quantity in the frequency domain that is related to the coupling coefficients in the generalised $n\tau$-law) is also amplitude-dependent, in addition to the time-lag. In this way, the FDF measurements in [6] are simulated more accurately, and as a result, the limit cycle amplitudes can be predicted well. Also, a plausible physical interpretation of the amplitude-dependence will be presented.

Our paper is structured in the following way. Section 2 is about the flame dynamics element, section 3 is about the burner acoustics element, and in section 4 the two elements are combined. The effects of the two nonlinear mechanisms will be investigated in section 5. Section 6 gives a tentative physical interpretation.

2. THE FLAME DESCRIBING FUNCTION

2.1. Measured results

Noiray et al. [19] studied a burner comprising effectively of an array of flames anchored by a perforated plate in the acoustic field of a quarter-wave resonator. They determined the "flame describing function" (FDF) experimentally by measuring the flame transfer

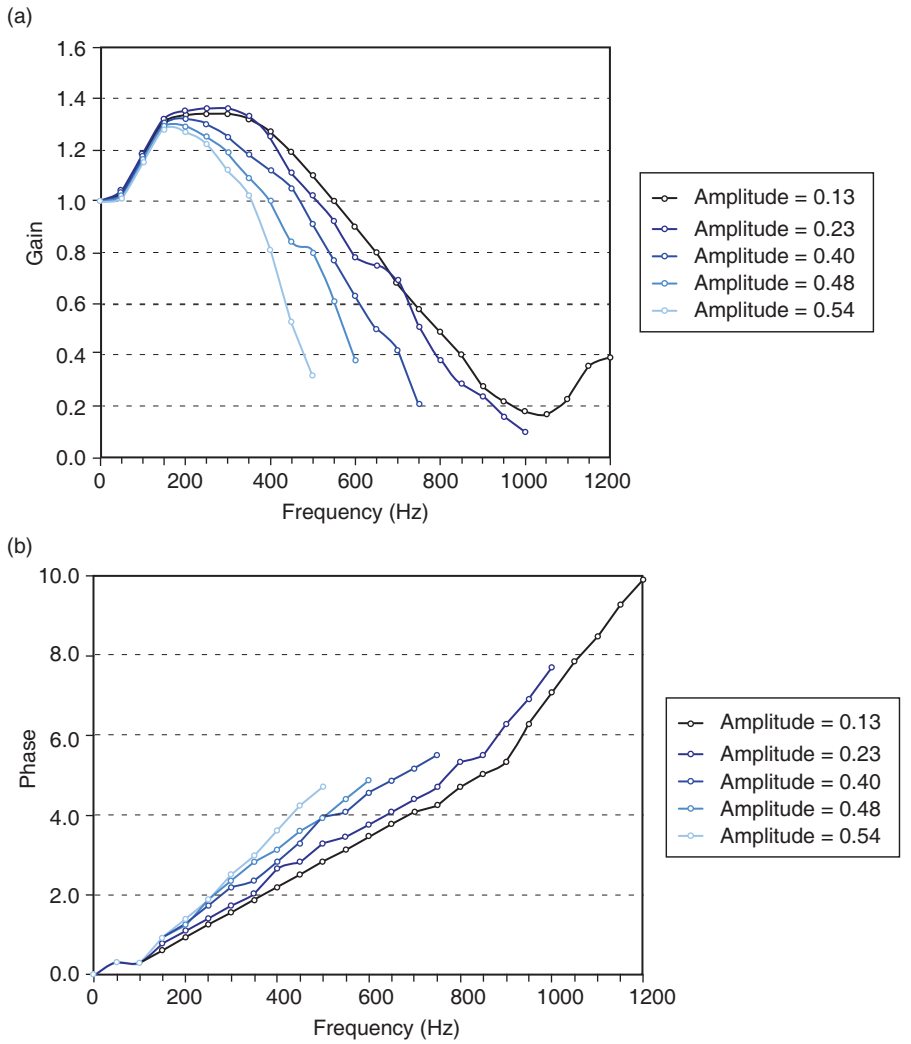

Figure 1: Measured FDF for different velocity amplitudes (normalised with the mean velocity) (a) gain. (b) phase.

function (FTF) for a range of velocity amplitudes. Their results for the gain and phase have been reproduced in Figures 1 (a, b).

The following features are notable.

(1) In the gain curves, there are two effects as the amplitude increases:
   (a) The frequency interval, which spans the first minimum (at zero frequency) to the next minimum becomes smaller.
   (b) The gain-maximum becomes smaller.

(2) The slope of the phase curves increases as the amplitude increases.

2.2. Analytical description

Our starting point is the hypothetical heat release law in the time domain,

$$\frac{Q(t)}{\bar{Q}} = n_1 \frac{u(t-\tau)}{\bar{u}} - n_0 \frac{u(t)}{\bar{u}} , \tag{2.1}$$

where

$\bar{Q}$: rate of heat release, mean part
Q: rate of heat release, fluctuating part
$\bar{u}$: velocity, mean part
u : velocity, fluctuating part
τ : time-lag
n_0, n_1: real positive parameters

This heat release law has a time-lagged component $u(t-\tau)$ and an instant component $u(t)$. It is based on physical and empirical reasoning: the analysis from first principles (kinematic description of the flame front by the G-equation) of a two-dimensional laminar V-flame predicts a rate of heat release proportional to $u(t-\tau) - u(t)$ [21]. We have added the parameters n_0 and n_1 with a view of finding suitable empirical values for them.

The frequency-domain equivalent of (2.1) is

$$\frac{\hat{Q}(\omega)}{\bar{Q}} = (n_1 e^{i\omega\tau} - n_0) \frac{\hat{u}(\omega)}{\bar{u}} , \tag{2.2}$$

which gives the FTF, $\mathcal{T}(\omega)$, as

$$\mathcal{T}(\omega) = n_1 e^{i\omega\tau} - n_0. \tag{2.3}$$

The gain of this FTF,

$$|\mathcal{T}(\omega)| = \sqrt{n_0^2 + n_1^2 - 2n_0 n_1 \cos\omega\tau} , \tag{2.4}$$

is a periodic function of $\omega\tau$ with a minimum at $\omega\tau = 0$, followed by a maximum at $\omega_{max}\,\tau = \pi$ and a subsequent minimum at $\omega_{min}\,\tau = 2\pi$.

The phase of this FTF is

$$\arg\mathcal{T}(\omega) = \frac{n_1 \sin\omega\tau}{n_1 \cos\omega\tau - n_0} \approx \frac{n_1}{n_1 - n_0}\omega\tau ; \tag{2.5}$$

the last step in (2.5) is an approximation for small frequencies, and this indicates that, at small frequencies, the slope of the phase curve is proportional to the time-lag τ.

In order to fit our analytical $\mathcal{T}(\omega)$ to the measured curves in Figure 1, we chose

$$n_1 - n_0 = 1 \text{ (this gives a gain of 1 at } \omega = 0) \tag{2.6a}$$

$$n_1 + n_0 = g_{max} \text{ (this gives a gain of } g_{max} \text{ at the 1st maximum)} \tag{2.6b}$$

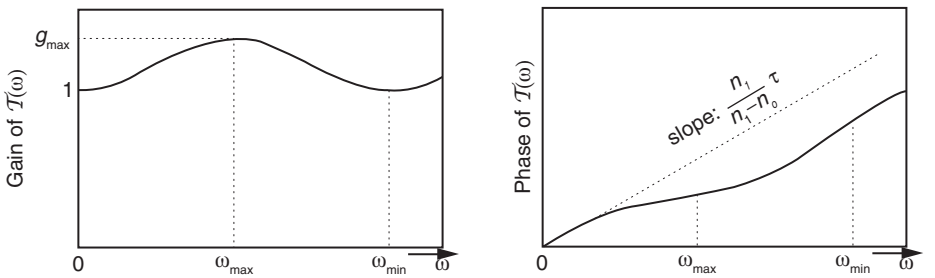

Figure 2: Analytical flame transfer function corresponding to equ. (2.3)

Table 1: FDF properties for increasing velocity amplitudes A.

$A/\bar{u}$	g_{max}	f_{min}[Hz]	$\tau[10^{-3}s]$
0.13	1.34	1050	0.95
0.23	1.36	1010	0.99
0.40	1.32	850	1.18
0.48	1.29	650	1.54
0.54	1.28	550	1.82

The gain measured at the smallest amplitude is shown by the black curve in Figure 1(a). For this curve, we have $g_{max} \approx 1.34$ and $\omega_{min} \approx 2\pi \cdot 1050 s^{-1}$. The latter result gives $\tau = 0.95 \cdot 10^{-3}$s. This agrees with the value obtained from the corresponding phase curve in Figure 1(b). At higher amplitudes, both the time-lag τ and the gain-maximum g_{max} change. The g_{max}- values can be read off Figure 1(a) directly, and the τ values can be estimated by extrapolating the gain curves to their second minimum. Table 1 shows the values for Noiray's five amplitudes.

The data in Table 1 has been used to generate Figures 3(a) and 3(b), which show the amplitude-dependence of the time-lag and of the gain-maximum, respectively.

The data points for the time-lag lie on a curve with growing slope. We approximate them analytically by a parabola, whose vertex is at the point $(0, \tau_0)$, i.e. by

$$\tau = \tau_0 + \tau_2 \left(\frac{A}{\bar{u}}\right)^2 . \tag{2.7}$$

For the constants τ_0 and τ_2 we chose

$$\tau_0 = 0.94 \cdot 10^{-3}s, \tau_2 = 2.5 \cdot 10^{-3}s, \tag{2.8a,b}$$

because this gives reasonable agreement with the measured data, as shown in Figure 3(a).

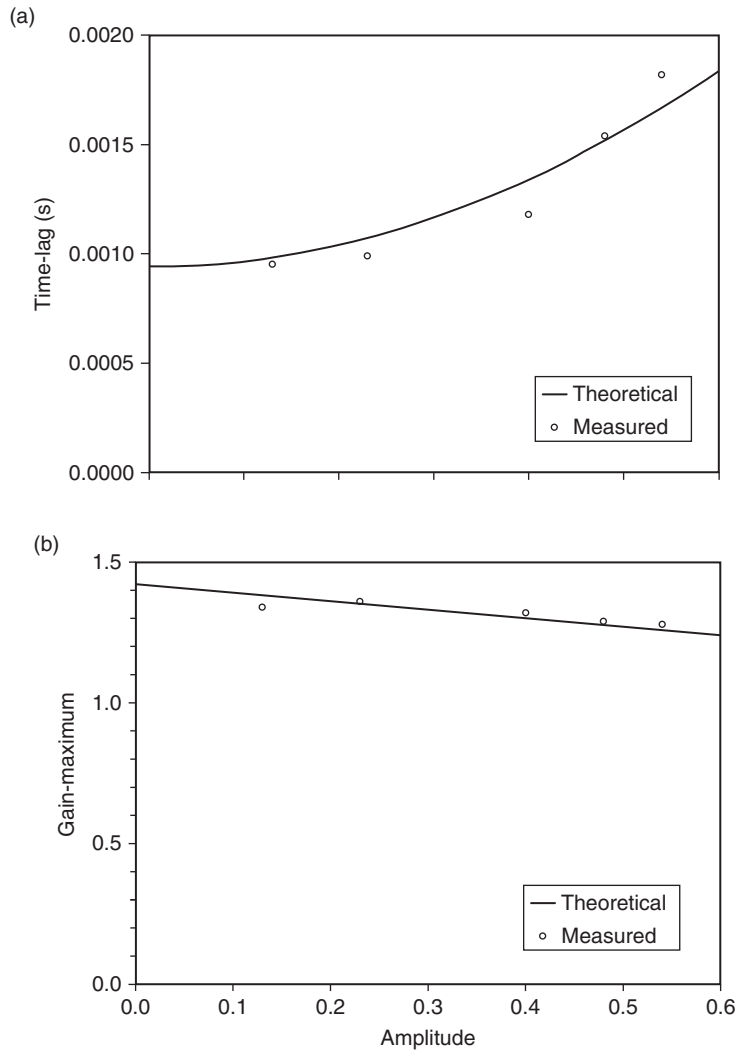

Figure 3: Dependence on velocity amplitude of (a) time-lag. (b) gain-maximum.

The data points for the gain-maximum are somewhat irregular, but show an overall decreasing trend. We approximate them analytically by a line with a negative slope, i.e. by

$$g_{\max} = g_0 - g_1 \frac{A}{\bar{u}} . \tag{2.9}$$

For the constants g_0 and g_1 we chose

$$g_0 = 1.42, g_1 = 0.3, \tag{2.10a,b}$$

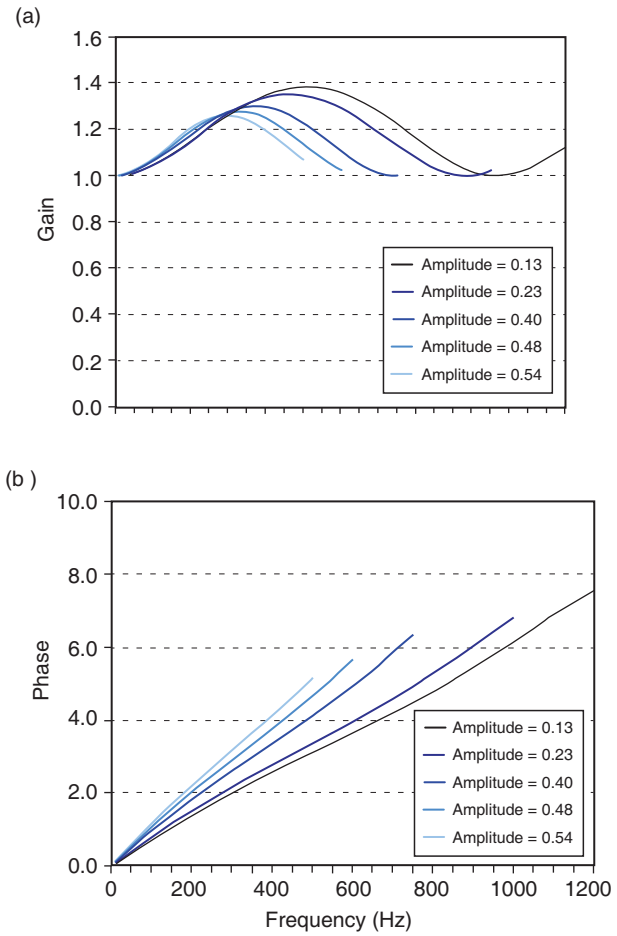

Figure 4: Analytical FDF. (a) gain. (b) phase.

because this gives reasonable agreement with the measured data, as shown in Figure 3(b).

Figure 4 shows the gain and phase of our analytical FDF, which is based on (2.3) and represented by

$$\mathcal{T}(\omega, A) = n_1(\mathrm{A})\mathrm{e}^{\mathrm{i}\omega\tau(A)} - n_0(A) \tag{2.11}$$

with

$$n_1(A) = \frac{1}{2}[g_{max}(A)+1]\,,\ n_0(A) = \frac{1}{2}[g_{max}(A)-1]\,. \tag{2.12a,b}$$

Incidentally, a correlation similar to (2.1), with amplitude-dependent time-lag and amplitude-dependent interaction index, has been determined experimentally for a turbulent flame in a combustor with choked inlet [15].

Comparison of Figure 4 with Figure 1 shows that our analytical representation captures the following key features of the measured FDF.

(1) The position of the maximum and subsequent minimum in the gain curves moves to smaller frequency values as the amplitude increases.
(2) The slope of the phase curve (which for small frequencies is proportional to τ) increases as the amplitude increases.
(3) The value of the gain-maximum decreases as the amplitude increases.

Not captured in our assumptions is the low-pass behaviour of the measured FDF, which leads to a reduction in gain at higher frequency values. Effectively, the overall gain in our model is an overestimation of the measured values.

3. THE COMBUSTION RIG DESCRIBED AS AN ACOUSTIC RESONATOR

3.1. Experimental setup

The experimental setup consists of a tube terminated at the upstream end by a piston with variable position and at the downstream end by a perforated plate, as shown schematically in Figure 5. A premixed gas (methane and air) enters the tube through small holes in the otherwise rigid piston. This mixture passes through the perforated plate, which acts as a flame holder, and is burnt in the matrix flame just outside the tube. Essentially, the tube is a quarter-wave resonator (one rigid and one nearly open end) with variable length L.

3.2. Theoretical model

We assume purely one-dimensional conditions, not only inside the tube, but also beyond its downstream end. The wave transmitted beyond this end is of course three-dimensional, but we ignore this and instead assume that the tube has a semi-infinite

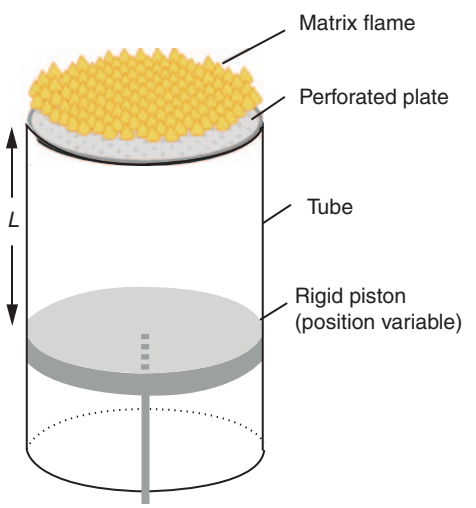

Figure 5: Noiray's matrix burner [19].

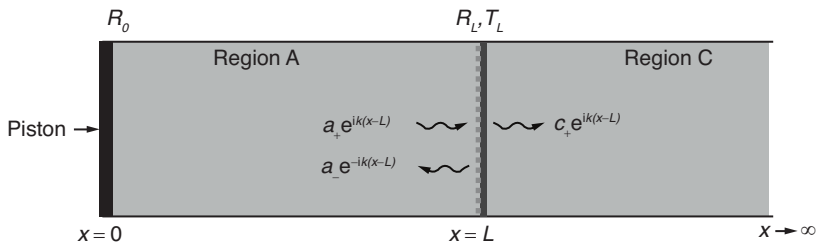

Figure 6: The modelled configuration. a_+, a_-, c_+ are pressure amplitudes.

continuation, which keeps the transmitted wave one-dimensional. This is shown in Figure 6. We also assume that the mean temperature and the speed of sound (denoted by c) are uniform everywhere.

The acoustic field inside the tube consists of backward and forward travelling waves with wave number $k = \omega/c$. These are reflected at the upstream end ($x = 0$) by the piston with reflection coefficient R_0, and at the downstream end ($x = L$) with reflection coefficient R_L. Waves are transmitted at the downstream end into the semi-infinite continuation with transmission coefficient T_L.

The downstream tube end is modelled as a pair of adjacent interfaces, one interface acting like a perforated plate and the other one like an open end. The reflection and transmission coefficients of a perforated plate are known,

$$R_{pp} = \frac{\omega}{\omega + 2\mathrm{i}\mathcal{N}cK} \quad \text{and} \quad T_{pp} = \frac{2\mathrm{i}\mathcal{N}cK}{\omega + 2\mathrm{i}\mathcal{N}cK}, \tag{3.1a,b}$$

(see [22] p. 361), where $\mathcal{N}$ is the number of holes per unit area, and K is the Rayleigh conductivity; for a plate of thickness h and with circular holes of radius r_p (see [22] p. 356),

$$K = \frac{r_p^2 \pi}{r_p \pi / 2 + h}. \tag{3.2}$$

The reflection coefficient of an unflanged open tube end with radius a is also known (see [24])

$$R_{oe} = -\frac{1 - \left[\frac{1}{4}\left(\frac{\omega a}{c}\right)^2 - \mathrm{i}\frac{\omega a}{c}0.6133\right]}{1 + \left[\frac{1}{4}\left(\frac{\omega a}{c}\right)^2 - \mathrm{i}\frac{\omega a}{c}0.6133\right]}. \tag{3.3}$$

In order to model the wave radiated from the open end, we construct a complex transmission coefficient, T_{oe}, in the following way: its magnitude guarantees acoustic energy conservation, i.e. $|R_{oe}|^2 + |T_{oe}|^2 = 1$, and its phase is such that the phase of the velocity is continuous at the tube end. This gives

$$T_{oe} = |T_{oe}|e^{i\varphi}, \text{ with } \left|T_{oe}\right| = \sqrt{1-\left|R_{oe}\right|^2} \text{ and } \varphi = \mathrm{Arg}(1-R_{oe}). \tag{3.4}$$

The reflection and transmission coefficient of the combined interface (perforated plate and open end) can be calculated as shown in [20]; the results are

$$R_L = \frac{R_{pp} - R_{pp}^2 R_{oe} + T_{pp}^2 R_{oe}}{1 - R_{pp} R_{oe}}, \tag{3.5}$$

$$T_L = \frac{T_{pp} T_{oe}}{1 - R_{pp} R_{oe}}. \tag{3.6}$$

The eigenfrequencies ω_n of this configuration are given by

$$F(\omega) = e^{-i\omega L/c} - R_0 R_L e^{i\omega L/c} = 0. \tag{3.7}$$

They are generally complex with a negative imaginary part.

We are going to use a Green's function approach, which requires the tailored Green's function, i.e. the impulse response of the acoustic resonator. This has been derived in [20] and is given by a superposition of modes n,

$$G(x, x', t, t') = \mathrm{H}(t-t') \sum_{n=1}^{\infty} \mathrm{Re}\left[G_n(x,x') e^{-i\omega_n (t-t')} \right], \tag{3.8}$$

where x, t are the observer coordinates (position and time), and x', t' are the source coordinates (position and time). $\mathrm{H}(t - t')$ is the Heaviside function (this guarantees causality), the amplitudes G_n are given by

$$G_n(x, x') = -\frac{c}{2L} R_0 \, T_L^2 \, e^{2i\omega_n (x + x')/c}. \tag{3.9}$$

4. THE COMBUSTION RIG WITH FLAME

4.1. Analytical stability criterion for a single mode

The mathematical steps in the derivation of the stability criterion are lengthy and complex; details can be found in [20]. Here we just give a few highlights.

The flame is assumed to be compact and situated at position x_q. We model it by

$$q(x, t) = q(t)\delta(x - x_q), \tag{4.1}$$

where $q(x, t)$ is the rate of heat release per unit mass (fluctuating part), and $q(t)$ is its time-dependent part; the delta-function describes its localised nature. $q(t)$ is related to the global heat release rate $Q(t)$ by

$$q(t) = \frac{Q(t)}{\bar{\rho}\mathcal{A}} = \alpha\left[n_1 u(t-\tau) - n_0 u(t)\right], \tag{4.2}$$

with $\alpha = \bar{Q}/(\bar{u}\,\bar{\rho}\,\mathcal{A})$, where $\bar{\rho}$ is the mean density and $\mathcal{A}$ is the cross-sectional area of the tube.

A Green's function approach is employed to derive an integral equation for the acoustic velocity. This is

$$u(t) = \frac{B}{2}\int_{t'=0}^{t}\sum_{n=1}^{\infty}\left[G_n e^{-i\omega_n(t-t')} + G_n^* e^{i\omega_n^*(t-t')}\right] q(t')\,dt', \tag{4.3}$$

where $B = -(\gamma - 1)/c^2$ is an abbreviation, and γ denotes the specific heat ratio. G_n is given by (3.9) with $x = x_q$ and $x' = x_q$, and G_n^* is its complex conjugate.

A single mode n can be considered by dropping the summation sign in (4.3). The resulting equation can be converted to an ODE for $u(t)$, and the result is

$$\ddot{u} - 2\mathrm{Im}(\omega_n)\dot{u} + |\omega_n|^2 u = -B\mathrm{Im}(\omega_n G_n^*)q(t) + B\mathrm{Re}(G_n)\dot{q}(t). \tag{4.4}$$

This is the ODE for a forced harmonic oscillator. It is the governing equation for the acoustic velocity $u(t)$, forced by the heat release rate $q(t)$ and its time derivative $\dot{q}(t)$. Substitution of (4.2) into (4.4) leads to

$$\ddot{u}(t) + c_1\dot{u}(t) + c_0 u(t) = b_0 u(t-\tau) + b_1\dot{u}(t-\tau), \tag{4.5}$$

with

$$b_0 = -\alpha n_1 B\,\mathrm{Im}(\omega_n G_n^*),\ b_1 = \alpha n_1 B\,\mathrm{Re}(G_n), \tag{4.6a,b}$$

$$c_0 = |\omega_n|^2 - \alpha n_0 B\,\mathrm{Im}(\omega_n G_n^*),\ c_1 = -2\,\mathrm{Im}(\omega_n) + \alpha n_0 B\,\mathrm{Re}(G_n). \tag{4.6c,d}$$

The time-lag is not necessarily small, in fact it can become larger than the period of the oscillation. We assume that $u(t)$ is sinusoidal with frequency Ω and amplitude A,

$$u(t) = A\cos\Omega t \tag{4.7}$$

and express the time-lag terms in terms of $u(t)$ and $\dot{u}(t)$. This gives

$$u(t-\tau) = A\cos\Omega(t-\tau) = (\cos\Omega\tau)\,u(t) - \frac{\sin\Omega\tau}{\Omega}\,\dot{u}(t), \tag{4.8}$$

$$\dot{u}(t-\tau) = (\Omega\sin\Omega\tau)\,u(t) + (\cos\Omega\tau)\,\dot{u}(t), \tag{4.9}$$

and (4.5) can then be written as

$$\ddot{u}(t) + \left[c_1 + b_0\frac{\sin\Omega\tau}{\Omega} - b_1\cos\Omega\tau\right]\dot{u}(t) + \left[c_0 - b_0\cos\Omega\tau - b_1\Omega\sin\Omega\tau\right]u(t) = 0. \tag{4.10}$$

Clearly, this is the equation for a damped harmonic oscillator. The damping coefficient is

$$a_1 = c_1 + b_0\frac{\sin\Omega\tau}{\Omega} - b_1\cos\Omega\tau\ , \tag{4.11}$$

and the other coefficient,

$$a_0 = c_0 - b_0\cos\Omega\tau - b_1\Omega\sin\Omega\tau \tag{4.12}$$

is the square of the oscillation frequency. The amplitude-dependence comes in through the time-lag (see (2.7)), which appears explicitly in (2.7), and indirectly through the gain-maximum (see (2.9)), which determines the coefficients n_0 and n_1 in (4.2). The damping coefficient is an indicator for the stability behaviour:

$$\begin{aligned} a_1 > 0 \quad & \text{stable} \\ a_1 < 0 \quad & \text{unstable} \end{aligned} \tag{4.13}$$

It is instructive to examine the values of a_1 for an array of parameter values for L and A. Contours of $a_1(L, A) = 0$ in the LA - plane indicate steady oscillations, i.e. limit cycles.

4.2. Measured and predicted stability behaviour

The parameters describing the combustion rig are:

$a = 0.035$m (tube radius)
$L = 0.1$m … 0.8m (range of tube lengths)
$h = 0.003$m (thickness of perforated plate)
$\mathcal{N} = 1.09 \cdot 10^5\text{m}^{-2}$ (number of perforations per unit area of plate)
$r_p = 0.001$m (radius of perforations)
$c = 345\text{ms}^{-1}$ (speed of sound)
$\gamma = 1.4$ (specific heat ratio)
$\alpha = 3\cdot 10^5\text{m}^2\text{s}^{-2}$ (factor relating $q(t)$ and $Q(t)$)

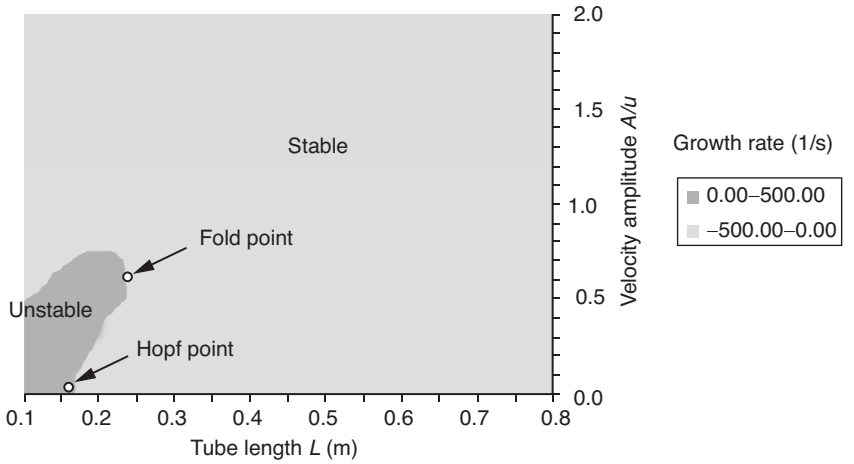

Figure 7: Measured stability map for mode 1.

$x_q - L = 0.01$m (distance of flame from perforated plate)
$R_0 = 1$ (pressure reflection coefficient at the piston)

We consider only the fundamental mode, $n = 1$, of the combustor. Its **measured stability map** is shown in Figure 7. Pale grey regions indicate stability, and dark grey regions indicate instability. In order to make it easy to compare this map with our predictions, which cover the amplitude range $A/\overline{u} = 0\ldots2$, we plotted Noiray's map for the same range. However, Noiray's data is available only for the range $A/\overline{u} = 0 \ldots 0.8$, so the "results" shown in Figure 7 for $A/\overline{u} > 0.8$ are not reliable.

The unstable region has the shape of a tongue. Linear stability behaviour can be discerned from the behaviour near the L-axis. The point $L = 0.17$m, $A/\overline{u} = 0$ on the map separates the linearly unstable and linearly stable range. This point is a subcritical Hopf bifurcation. Branching off from this point are unstable limit cycles. The point $L = 0.24$m, $A/\overline{u} = 0.5$, i.e. the "tip of the tongue", is a fold point. It separates unstable limit cycles from stable ones. The region between $L = 0.17$m and $L = 0.24$m is a bi-stable region, where hysteresis can be observed.

The **predicted stability maps** are shown in Figure 8 and Figure 9 (they are on the same scale as Figure 7). There were produced by evaluating the damping coefficient (4.11) for the combustion rig described by the parameter values at the beginning of this section. The FDF was calculated as described in section 2.2. It contains 4 parameters: τ_0, g_0, τ_2, g_1. The first two, τ_0 and g_0, determine the linear behaviour. We kept them fixed at the optimal values found in section 2.2: $\tau_0 = 0.94 \cdot 10^{-3}$ s and $g_0 = 1.42$. The other two parameters, τ_2 and g_1, specify the amplitude-dependence of the time-lag (see (2.7)) and of the gain-maximum (see (2.9)), respectively; they determine the nonlinear behaviour. For τ_2, we choose again the optimal value found in section 2.2: $\tau_2 = 2.5 \cdot 10^{-3}$ s.

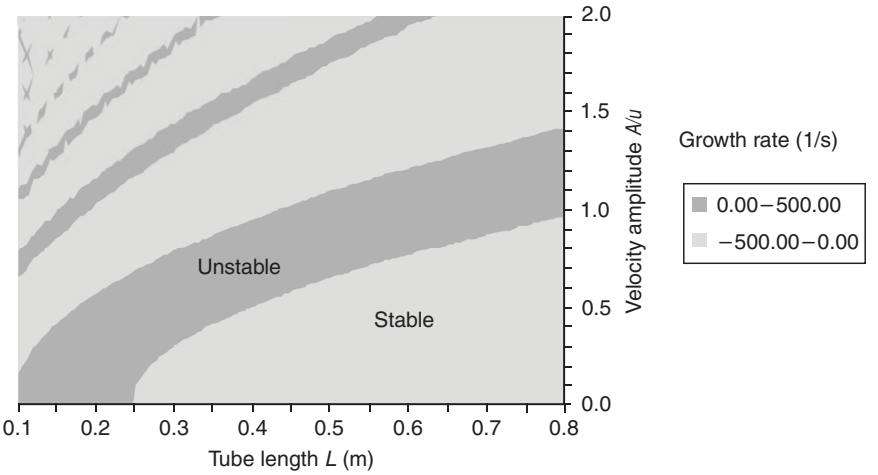

Figure 8: Predicted stability map for $\tau_0 = 0.94 \cdot 10^{-3}$s, $g_0 = 1.42$, $\tau_2 = 2.5 \cdot 10^{-3}$s, $g_1 = 0.3$.

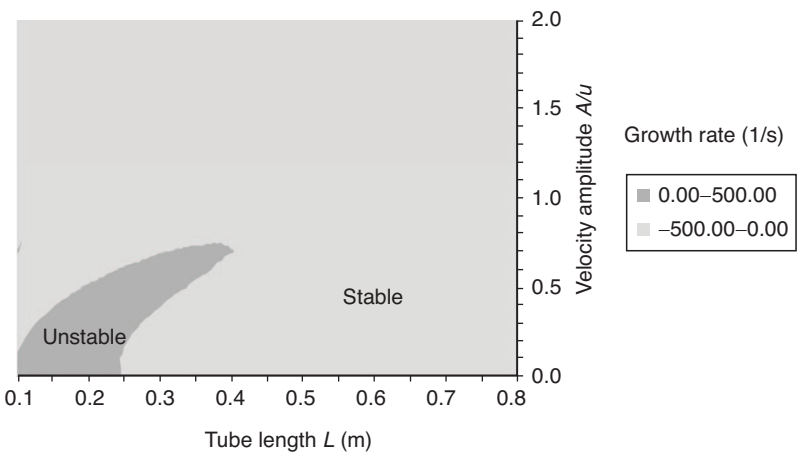

Figure 9: Predicted stability map for $\tau_0 = 0.94 \cdot 10^{-3}$s, $\tau_2 = 2.5 \cdot 10^{-3}$s, $g_1 = 1.0$.

The optimal value for g_1 was found to be $g_1 = 0.3$. This results in the stability map shown in Figure 8. The unstable regions have the shape of a curved band. There is a main band, and above that, there are several minor bands with decreasing width.

These predictions capture the behaviour at low amplitudes, in particular the linear stability range and the limit cycle amplitudes for low L -values. However, there is a major discrepancy: our model predicts a *band* of instability, which spans the whole

L -range, whereas Noiray's instability region has the shape of a *tongue*, which does not extend beyond L -values of 0.25 m. Put in nonlinear dynamics terms, we predict the subcritical Hopf bifurcation point correctly, but fail to capture the fold point.

If the parameter g_1 is chosen to be $g_1 = 1.0$, instead of 0.3, the stability map looks quite different, as shown in Figure 9. The unstable region now has the shape of a (single) tongue with all the qualitative features as its measured counterpart in Figure 7.

The excellent qualitative agreement between the measured map in Figure 7 and the predicted map in Figure 9 indicates that our model works well, albeit with an artificially high g_1- value. Increasing the g_1- value amounts to reducing the overall gain. It is not surprising that we had to do that: with an artificially reduced gain we are effectively compensating for the fact that we overestimated the gain earlier when we ignored the low-pass behaviour of the FDF.

The linear regime in the stability maps is given by the behaviour along the L - axis, i.e. the behaviour at zero amplitude. In our predictions we have

instability if $0.1\text{m} < L < 0.24\text{m}$
stability if $0.24\text{m} < L < 0.8\text{m}$

These ranges are determined by the parameters τ_0 and g_0 in the FDF.

In the next section we will systematically explore the effect of the coefficients τ_2 and g_1, which specify the amplitude-dependence of the FDF and are responsible for the nonlinear behaviour.

5. EFFECT OF THE NONLINEARITIES CAPTURED BY THE FLAME DESCRIBING FUNCTION

The figures that will be shown in this section are smaller than those in the previous section. However, comparison is still possible as the new figures cover the same L and A range as Figures 7 to 9, and have the same aspect ratio.

5.1. Amplitude-dependent time-lag

In this section, we consider the case, where the time-lag depends on amplitude as specified in (2.7), with $\tau_0 = 0.94 \cdot 10^{-3}$s and variable τ_2. The gain-maximum is kept constant with $g_0 = 1.42$ and $g_1 = 0$ in (2.9).

Figure 10 shows the stability maps for the following eight cases:

$\tau_2 = -0.2 \cdot 10^{-3}$ s, 0s, $0.2 \cdot 10^{-3}$ s, $0.4 \cdot 10^{-3}$ s in the top row, and

$\tau_2 = -0.6 \cdot 10^{-3}$ s, $0.8 \cdot 10^{-3}$ s, $1.0 \cdot 10^{-3}$ s, $2.0 \cdot 10^{-3}$ s in the bottom row.

$\tau_2 = 0$ describes a constant time-lag, $\tau_2 > 0$ describes a time-lag that increases with amplitude, and $\tau_2 < 0$ one that decreases. For $\tau_2 = 0$, the region of instability is a rectangular band that spans the whole amplitude range (see 2nd map in the top row). For negative τ_2, e.g. $\tau_2 = -0.2 \cdot 10^{-3}$ s (see 1st map in the top row), the instability band curves to the left, giving rise to a bifurcation point along the L - axis, which is a *super*critical Hopf point; however, this scenario is not of interest. The interesting scenario is the case of positive τ_2 because this was actually observed. The remaining six maps in Figure 10 show the following developments as τ_2 increases from zero:

The rectangular band curves to the right and flares towards the top. The curvature increases, and the band spans a larger and larger L -range. In addition, minor bands appear above the main band. Their number increases, and they, too, span a larger and

larger L - range. The bifurcation point along the L - axis is a *sub*critical Hopf point; there is no sign of a fold point appearing.

5.2. Amplitude-dependent gain-maximum

We now consider the case, where the gain-maximum depends on amplitude as specified in (2.9), with $g_0 = 1.42$ and variable g_1. The time-lag is kept constant with $\tau_0 = 0.94 \cdot 10^{-3}$ s and $\tau_2 = 0$ in (2.7).

Figure 11 shows the stability maps for the following eight cases:

$g_1 = -0.2, 0, 0.2, 0.4$ in the top row, and

$g_1 = 0.6, 0.8, 1.0, 2.0$ in the bottom row.

$g_1 = 0$ describes a constant gain-maximum, $g_1 > 0$ describes a gain-maximum that decreases with amplitude, and $g_1 < 0$ one that increases. For $g_1 = 0$, the region of instability is a rectangular band that spans the whole amplitude range (see 2nd map in the top row). For negative g_1, e.g. $g_1 = -0.2$ (see 1st map in the top row), the instability band, becomes wider towards the top, giving rise to a bifurcation point along the L - axis, which is a *sub*critical Hopf point; however, this scenario is not of interest.

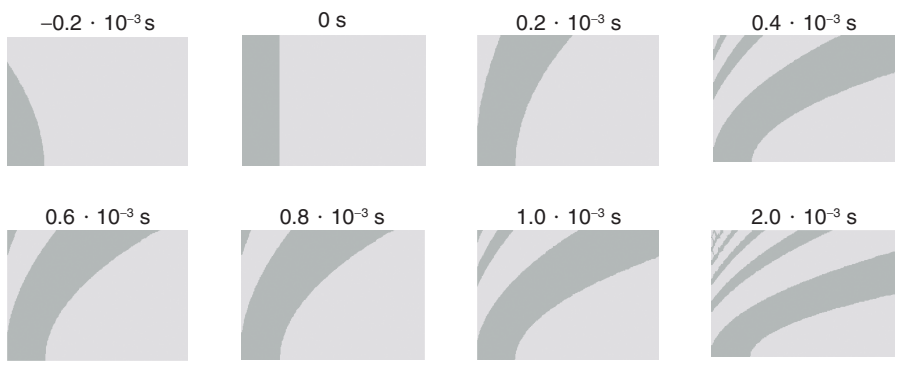

Figure 10: Stability maps for various values of τ_2, and $g_1 = 0$.

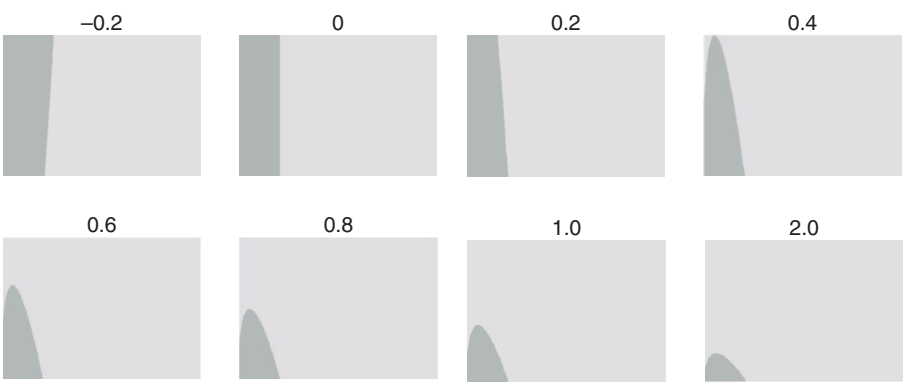

Figure 11: Stability maps for various values of g_1, and $\tau_2 = 0$.

The interesting scenario is the case of positive g_1 because this was actually observed. The remaining six maps in Figure 11 show the following developments as g_1 increases from zero:

The instability band becomes narrower towards the top, and eventually it takes the shape of a vertically pointing tongue. The bifurcation point along the L - axis is a *super*critical Hopf point; there is no sign of a fold point appearing.

5.3. Amplitude-dependent time-lag and gain-maximum

We now consider the case where both, the time-lag *and* the gain-maximum, depend on amplitude, as specified in (2.7) and (2.9), with $\tau_0 = 0.94 \cdot 10^{-3}$ s and $g_0 = 1.42$. We keep τ_2 constant at $\tau_2 = 2.5 \cdot 10^{-3}$ s, and vary g_1.

Figure 12 shows the stability maps for the following eight cases:

$g_1 = 0, 0.3, 0.4, 0.6$ in the top row, and

$g_1 = 1.0, 2.0, 3.0, 4.0$ in the bottom row.

The eight maps in Figure 12 show the following developments as g_1 increases from zero:

Initially (see 1st map in top row), there is a main band of instability with several minor bands above it. The bifurcation point along the L - axis is a subcritical Hopf point. All bands curve to the right and flare. In subsequent maps, the minor bands fade away, and eventually they disappear altogether (see the four maps in the lower row). The main band develops into a tongue, which points to the right (between $g_1 = 0.6$ and 1), giving rise to a fold point and a bistable region (see 1st map in bottom row). If g_1 is increased further, the tongue becomes shorter and more vertical, and eventually the fold point, together with the bistable region, disappears. As the fold point disappears, the bifurcation point along the L -axis turns into a supercritical Hopf point.

Our simulations also showed that both time-lag *and* gain-maximum must be amplitude-dependent; the time-lag on its own fails to predict the observed fold point.

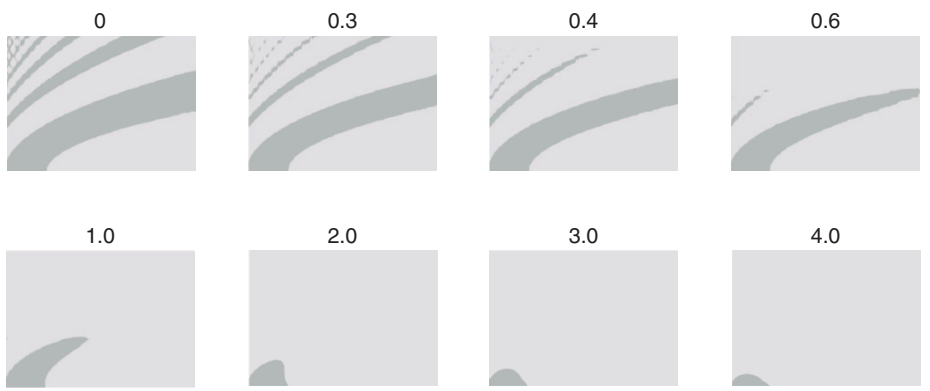

Figure 12: Stability maps for various values of g_1, and $\tau_2 = 2.5 \cdot 10^{-3}$ s.

6. SUMMARY AND TENTATIVE INTERPRETATION

We considered a specific combustion rig as a system of two coupled elements: an acoustic resonator and a flame with oscillating rate of heat release. We described the acoustics of the combustion rig in terms of modes, and derived a governing equation for one such mode. This turned out to be the equation for a damped harmonic oscillator, forced by the heat release rate from the flame. In order to model the heat release rate, and in particular its nonlinear aspects, we developed a generalised $n\tau$ -law,

$$\frac{Q(t)}{\bar{Q}} = n_1 \frac{u(t-\tau)}{\bar{u}} - n_0 \frac{u(t)}{\bar{u}}, \tag{6.1}$$

with amplitude-dependent coefficients τ, n_0, n_1. The representation of (6.1) in the frequency domain leads to the FDF

$$\mathcal{T}(\omega, A) = n_1(A) e^{i\omega\tau(A)} - n_0(A) . \tag{6.2}$$

The coefficients and their amplitude-dependence were determined by matching the gain and phase of this FDF to measured values. The gain and phase of this analytical FDF agree well with the measured gain and phase.

Two aspects of this approach are worth being highlighted: multiple time-lags and amplitude-dependence.

6.1. Multiple time-lags

Our heat release law involves the time-lagged velocity $u(t-\tau)$, and also the instantaneous velocity $u(t)$. We have shown in this paper that the excess observed in the gain spectrum of the FTF is a direct consequence of this superposition. The inclusion of the $u(t)$ term in the heat release law may seem new, but in fact it has been touched upon by some earlier researchers.

In his studies of a single conical flame [24], Kornilov proposed a "phenomenological fit function" for the FTF. This features the superposition of a $e^{i\omega\tau}$ term (which corresponds to $u(t-\tau)$) and a frequency-independent, i.e. constant, term (which corresponds to $u(t)$). The time-lag term is attributed to the flame kinematics, and the constant term to the oscillating heat loss from the flame base [25]. Kornilov observes excess gain in this FTF. In a later study, Kornilov et al [26] examine a multi-slit burner, which is the two-dimensional equivalent of the matrix flame. Again, excess gain is observed, and it is proposed that the motion of the flame anchoring point is responsible for that. Altay et al [27] have developed a detailed theoretical model, which includes the coupled effects of flame kinematics and heat loss from the flame base. Again, they find that the FTF exhibits excess gain; also, the position and height of the gain maximum depends on various parameters, such as the equivalence ratio. These findings suggest the following speculative interpretation from our side. The heat release rate from a matrix flame can be described by a superposition of

- a time-lagged velocity term, which describes the convective effects along the moving flame surface, and
- an instantaneous velocity term, which describes the heat losses at the flame bases, where convection plays no role.

6.2. Amplitude-dependence

The multiple time-lag aspects are purely linear. The nonlinearity comes in through the amplitude-dependence of the time-lag and of the gain-maximum. If this dependence is such that the time-lag *increases* and the gain maximum *decreases* with amplitude, the combustion rig is susceptible to dangerous limit cycles, i.e. limit cycles that have large amplitude and occur suddenly, when a linear analysis would suggest that the combustion rig is stable.

An explanation why the time-lag and gain maximum should be dependent on the excitation amplitude can be gathered from flame images taken at various points during one cycle of the imposed velocity field.

At low amplitudes, the flames are conical with a stationary flame base and smoothly elongating surface, i.e. the flame height oscillates harmonically, in phase with the imposed velocity oscillations. At high amplitudes, this behaviour changes significantly. The flame base is no longer stationary, but lifts and oscillates vertically [16]. Each flame no longer moves like a periodically elongating cone, but undergoes more complicated distortions. These have been observed in detail by Lang [17], who gave a phenomenological explanation, based on snapshots of flames taken at various points during a velocity cycle. During the low-velocity part of the cycle, the flames are short, and their bases are close to the perforated plate. As the velocity increases and reaches its maximum value, the flames elongate and the rate in heat release rises. However, as the velocity decreases, the flame tip is unable to adapt instantaneously to the new flow conditions. This is because the flame now has to move towards the flow, but it can do so only with the laminar flame speed, which is too small to keep up with the flow. This leads to flame pinching, followed by the separation of a flame pocket from the rest of the flame. The gas in each pocket is consumed quickly, leaving short flames as the velocity reaches its minimum, and a new cycle begins.

How do these observations relate to the amplitude-dependence of the time-lag and the gain maximum? The time-lag is associated with convection, covering the stand-off distance (i.e. the distance between the top surface of the perforated plate and the flame base) and some way up a flame cone. Since the stand-off distance increases with amplitude, the time-lag increases as well. The flame foot oscillations are also likely to play a role in this [16]. The gain maximum is a measure for the heat release rate during one cycle of the oscillation. The flame pinching and subsequent formation of flame pockets leads to a relatively small variation in the flame surface area, compared with the periodically elongating flame cone that is observed at low amplitudes. This leads to a reduction of the gain maximum with growing amplitude.

The explanations in this section are somewhat speculative and could be substantiated (or otherwise) by further studies of the dynamics of matrix flames at high excitation amplitudes.

REFERENCES

[1] Candel, S. Combustion dynamics and control: Progress and challenges. *Proceedings of the Combustion Institute,* 2002, 29, 1–28.

[2] Lieuwen, T. Modeling premixed combustion-acoustic wave interactions: A review. *Journal of Propulsion and Power,* 2003, 19, 765–781.

[3] Culick, F.E.C. Unsteady motions in combustion chambers for propulsion systems, published on CD, 2006, RTO-AG-AVT-039.

[4] Lieuwen, T., McDonell, V., Petersen, E. and Santavicca, D. Fuel flexibility influences on premixed combustor blowout, flashback autoignition and stability. *Journal of Engineering for Gas Turbines and Power - Transactions of the ASME*, 2008, 130

[5] Huang, Y. and Yang, V. Dynamics and stability of lean-premixed swirl stabilized combustion. *Progress in Energy and Combustion Science,* 2009, 35, 293–364.

[6] Noiray, N., Durox, D., Schuller, T. and Candel, S. A unified framework for nonlinear combustion instability analysis based on the flame describing function. *Journal of Fluid Mechanics,* 2008, 615, 139–167.

[7] Palies, P., Durox, D., Schuller, T. and Candel, S. Experimental study on the effect of swirler geometry and swirl number on flame describing functions. *Combustion Science and Technology,* 2011, 183, 704–717.

[8] Boudy, F., Durox, D., Schuller, T. and Candel, S. Analysis of limit cycles sustained by two modes in the flame describing function framework. *Comptes Rendus Mecanique,* 2013, 341, 181–190.

[9] Dowling, A.P. Nonlinear self-excited oscillations of a ducted flame. *Journal of Fluid Mechanics,* 1997, 346, 271–290.

[10] Dowling, A. P. A kinematic model of a ducted flame. *Journal of Fluid Mechanics,* 1999, 394, 51–72.

[11] Krediet, H.J., Beck, C.H., Krebs, W. and Kok, J.B.W. Saturation mechanism of the heat release response of a premixed swirl flame using LES. *Proceedings of the Combustion Institute,* 2013, 34, 1223–1230.

[12] Jaensch, S., Bomberg, S., Selimefindigil, F. and Polifke, W. Nonlinear identification of the flame describing function of a laminar premixed flame. *Proceedings of the n3l International Summer School and Workshop on Non-Normal and Nonlinear Effects in Aero- and Thermoacoustics, Munich, Germany, 18-21 June 2013*

[13] Crocco, L. Aspects of combustion stability in liquid propellant rocket motors Part 1: Fundamentals. *Journal of the American Rocket Society,* 1951, 21, 163–178.

[14] Raun, R.L., Beckstead, M.W., Finlinson, J.C. and Brooks, K.P. A review of Rijke tubes, Rijke burners and related devices. *Progress in Energy and Combustion Science,* 1993, 19, 313–364.

[15] Hield, P.A., Brear, M.J. and Jin, S.H. Thermoacoustic limit cycles in a premixed laboratory combustor with open and choked exits. *Combustion and Flame,* 2009, 156, 1683–1697.

[16] Durox, D., Schuller, T., Noiray, N. and Candel, S. Experimental analysis of nonlinear flame transfer functions for different flame geometries. *Proceedings of the Combustion Institute,* 2009, 32, 1391–1398.

[17] Lang, W. *Dynamics and stability of self-excited combustion oscillations when several frequencies are present. An extended stability criterion (in German).* PhD thesis, Technische Universität München, 1986.

[18] Noiray, N., Durox, D., Schuller, T. and Candel, S. Self-induced instabilities of premixed flames in a multiple injection configuration. *Combustion and Flame,* 2006, 145, 435–446.

[19] Noiray, N. *Linear and nonlinear analysis of combustion instabilities, application to multipoint injection systems and control strategies*. PhD thesis, École Centrale Paris, Laboratory EM2C, 2007.

[20] Heckl, M.A. Analytical model of nonlinear thermo-acoustic effects in a matrix burner. *Journal of Sound and Vibration,* 2013, 332, 4021–4036.

[21] Kosztin, B. "Small-amplitude nonlinear thermoacoustic oscillations". Private communication, April 2012.

[22] Howe, M.S. *Acoustics of fluid-structure interaction*. Cambridge University Press, Cambridge, 1998.

[23] Levine, H. and Schwinger, J. On the radiation of sound from an unflanged circular pipe. *Physical Review,* 1948, 73, 383–406.

[24] Kornilov, V.N. *Experimental research of acoustically perturbed Bunsen flames*. PhD thesis, Technische Universiteit Eindhoven, 2006.

[25] Manohar *Thermo-acoustics of Bunsen type premixed flames*. PhD thesis, Technische Universiteit Eindhoven, 2011.

[26] Kornilov, V.N., Rook, R., ten Thije Boonkkamp, J.H.M. and de Goey, L.P.H. Experimental and numerical investigation of the acoustic response of multi-slit Bunsen burners. *Combustion and Flame,* 2009, 156, 1957–1970.

[27] Altay, H.M., Park, S., Wu, D., Wee, D., Annaswamy, A.M. and Ghoniem, A.F. Modeling the dynamic response of a laminar perforated-plate stabilized flame. *Proceedings of the Combustion Institute,* 2009, 32, 1359–1366.